Effect of a static field on the stochastic layer of microwave-driven hydrogen

S. Cocke and L. E. Reichl

Center for Statistical Mechanics, University of Texas at Austin, Austin, Texas 78712

We study the effect of a static field on the stochastic layer of microwave-driven hydrogen using two approaches. We use the Chirikov overlap criterion on the Hamiltonian to estimate the critical field strength required for global chaos. We then derive the whisker and standard maps for this system valid for arbitrary field strengths and use the standard map to obtain a second estimate for the onset of global chaos. The standard-map estimate agrees well with both strobe plots and the whisker map plots for this system. Throughout, we use parameter values typically found in experiments.

I. INTRODUCTION

The hydrogen atom in a microwave field has become an important system in which to study the manifestation of chaos in quantum dynamics because it is analytically tractable and experimentally feasible. One-dimensional classical models, such as the SSE (Ref. 1) (surface-state electron) or "stretched hydrogen atom"[2] have been successful in explaining much of the fundamental dynamics of the hydrogen atom observed in recent experiments.[3] Most theoretical analyses to date, however, neglect the effect of a static (dc) electric field which is present in some experiments. The effects of a static field have been studied using classical dynamics by Stevens and Sundaram.[4] They include the static field by means of a dipole coupling of the static field in the Hamiltonian and construct action-angle variables to treat the microwave perturbation. Their analysis is valid for orbits that are weakly affected by the static field. In this paper, we will also treat the problem classically but we will include orbits that are strongly affected by the dc field, i.e., orbits which are near the potential turnover created by the static field. As in Stevens and Sundaram[4] and Jensen,[1] we will use the simple Chirikov overlap criterion[5] to determine the onset of chaos, and hence ionization. However, we will go further and derive the whisker map and standard map for arbitrary Stark field and will compare the estimates for onset of chaos given by the Chirikov overlap criterion to the results which we obtain from the more accurate predictions based on the standard map.

In this paper we consider a one-dimensional hydrogen atom in the presence of a static dc field and a microwave field, both of which couple to the electron in the hydrogen atom via a dipole interaction. In terms of atomic units the Hamiltonian for this system can be written

$$H = \tfrac{1}{2}p^2 - \frac{1}{x} - F_0 x - F x \cos(\omega t) , \qquad (1.1)$$

where p and x are the momentum and position of the electron, t is the time, F_0 and F are the strengths of the dc and microwave fields, respectively, and ω is the radial frequency of the microwave field.

II. CANONICAL TRANSFORMATION

Let us first consider a hydrogen atom in the presence of a constant field, $F_0 > 0$. The Hamiltonian can be written

$$H_0 = \tfrac{1}{2}p^2 - \frac{1}{x} - F_0 x = E_0 , \qquad (2.1)$$

where E_0 is the energy. Figure 1 shows a plot of the potential energy, $V(x) = -1/x - F_0 x$ versus x, the position of the electron. The potential energy has a turnover point at position $x^* = (1/F_0)^{1/2}$ and energy $E_0^* = -2(F_0)^{1/2}$. For a particle with energy $E_0 < E_0^*$ and $x < x^*$ (trapped in the potential well) the inner and outer turning points of the orbit are at $x = 0$ and $x = x_-$, respectively, while the turning point for a "free" electron with energy $E_0 < E_0^*$ impinging on the ionized atom is $x = x_+$, where

$$x_\pm = \frac{|E_0|}{2F_0} \left[1 \pm \left[1 - \frac{4F_0}{|E_0|^2} \right]^{1/2} \right] \qquad (2.2)$$

For the case when the electron is in a bound state ($x < x^*$) we can make a canonical transformation from variables (p,x) to action-angle variables (J,θ). The action
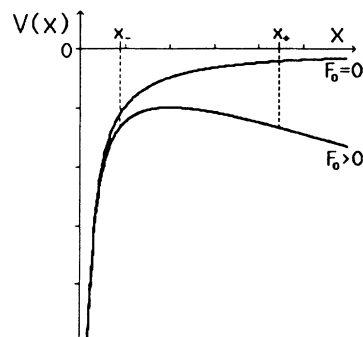

FIG. 1. Plot of the potential energy, $V(x) = -1/x - F_0 x$ for both $F_0 = 0$ and $F_0 \neq 0$.

is given by

$$J = \frac{1}{2\pi} \oint p \, dx = \frac{2\sqrt{2}[(1+k^2)E(k)-(1-k^2)K(k)]}{3\pi F_0^{1/4}k^{3/2}} .$$

(2.3)

The Hamiltonian $H_0 = H_0(J) = E_0$ cannot be written explicitly but is contained implicitly in Eq. (2.3). The angle variable can be found from Hamilton's equation $\dot{\theta} = \partial H_0/\partial J$ and is given by

$$\theta = \frac{\pi F_0^{3/4}k^{1/2}t}{\sqrt{2}[K(k)-E(k)]} ,$$

(2.4)

where $E(k)$ and $K(k)$ are the elliptic integrals of the first and second kind, respectively, and k is the modulus defined $k^2 = x_-/x_+$.

The canonical transformation between coordinates (p,x) and action-angle variables (J,θ) can be found by integrating the equation

$$\dot{x} = p = \pm[2(E_0 + 1/x + F_0 x)]^{1/2} .$$

(2.5)

We find

$$x = x_- \, \text{sn}^2(u,k) ,$$

(2.6)

where

$$u - E(u,k) = \frac{[E(k)-K(k)]\theta}{\pi} = \pm\frac{(F_0)^{1/2}t}{\sqrt{2}} .$$

(2.7)

In Eqs. (2.6) and (2.7), sn is a Jacobi elliptic function and $E(u,k)$ is the incomplete elliptic integral of the second kind. The dependence of x and p on J is given implicitly by Eqs. (2.3) and (2.6) via the modulus k.

III. ONSET OF CHAOS— CHIRIKOV OVERLAP CRITERION

Conditions for the onset of chaos can be determined from the Chirikov overlap criterion.[5] In order to use the Chirikov criterion, we must first expand the Hamiltonian in terms of the infinite set of traveling cosine waves which generate the nonlinear resonances in this system. After the canonical transformation to action-angle variables, the Hamiltonian Eq. (1.1) takes the form

$$H = H_0(J) - Fx(J,\theta)\cos(\omega t) ,$$

(3.1)

where $x(J,\theta)$ is a periodic function of θ. Following the recipe in Ref. 1, let us expand $x(J,\theta)$ in a Fourier series in θ. Then we have

$$H = H_0(J) - F\sum_{m=0}^{\infty} x_m(J)\cos(m\theta)\cos(\omega t) ,$$

(3.2)

where

$$x_m(J) = \frac{1}{2\pi}\int_0^\pi d\theta \, x(J,\theta)\cos(m\theta) .$$

(3.3)

In Fig. 2, $x_m(J)$ is plotted as a function of k, the modulus, for the range $k=0$ to $k=1$. When $k=0$ this corresponds to no static field being present and the coefficients x_m reduce to $x_m = J^2 J_m'(m)/m$ where
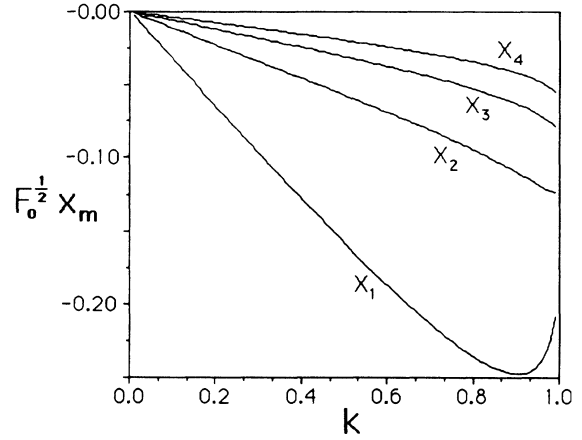

FIG. 2. A plot of the first four Fourier coefficients, $(F_0)^{1/2}x_m$, as a function of the modulus k, for $m = 1,2,3,4$.

$J_m'(z) = dJ_m(z)/dz$ and $J_m(z)$ denotes the Bessel function of order m.[1] An expression for $k \approx 1$ is derived later in this section.

We can rewrite Eq. (3.2) as

$$H = H_0(J) - \frac{F}{2}\sum_{m=-\infty}^{\infty} x_m(J)\cos(m\theta - \omega t) .$$

(3.4)

The perturbation may then be seen as a series of traveling wave potentials which may trap an electron traveling at nearly the same relative velocity, giving rise to nonlinear resonance zones in the phase space of the system. This yields a resonance condition $\dot{\theta} = \omega/m$. Since $\dot{\theta} = \partial H/\partial J \approx \partial H_0/\partial J$ for small F, our condition of resonance is

$$\frac{\omega}{m} \approx \frac{\pi F_0^{3/4}\sqrt{k}}{\sqrt{2}[K(k)-E(k)]} .$$

(3.5)

A plot of the action of the first primary resonance $(m=1)$ versus frequency is given in Fig. 3 for various dc field strengths. Note that increasing the dc field strength lowers (in action) the location of the resonances, especially for lower frequencies. At higher frequencies there is
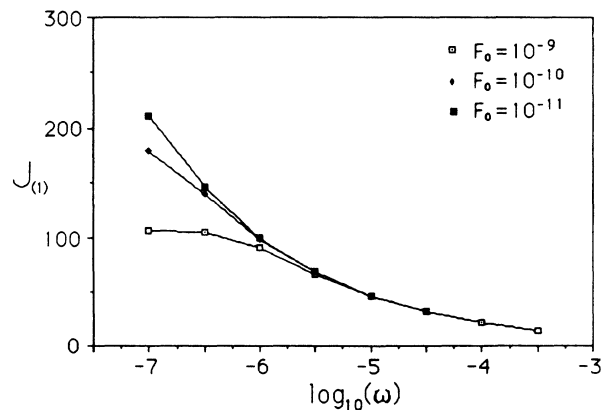

FIG. 3. A plot of the action, $J_{(1)}$, of the first primary resonance vs microwave frequency for three typical dc field strengths used in experiments.

little shift, as expected, since those frequencies correspond to more tightly bound electrons. Strobe plots of this system in (J, θ) space are given in Fig. 4 for two typical dc field strengths. The first and second primary resonances are clearly visible, as well as some secondary resonances which are generated by the primary resonances. The lowering of the resonances as the dc field strength increases is apparent and their location is correctly predicted by Eq. (3.5). In particular, Eq. (3.5) gives $J = 82.6$ and 96.5 for the first and second resonances, respectively, for $F_0 = 10^{-9}$.

The width of the resonances depends on the microwave and dc field strengths. To estimate this width we may try to use the pendulum approximation. To do this, first expand the Hamiltonian in a Taylor series about, say, the mth resonance and keep only the contribution from the mth traveling cosine (with positive velocity)

$$H = H_0(J_m) + \left[\frac{\partial H_0}{\partial J} \right]_{J_m} (J - J_m)$$

$$+ \frac{1}{2} \left[\frac{\partial^2 H_0}{\partial J^2} \right]_{J_m} (J - J_m)^2 - \frac{F}{2} x_m(J_m)\cos(m\theta - \omega t) \ .$$

$$(3.6)$$

$$\Delta I_m = 4 \left[F\frac{x_m}{2} \right]^{1/2} \left[\frac{-\pi^2 F_0 k^2 [(1+k^2)E(k) - (1-k^2)E(k)]}{4(1-k^2)^2 [K(k) - E(k)]^3} \right]^{-1/2} \ . \tag{3.10}$$

We can apply the resonance condition, Eq. (3.5), to obtain a simpler expression,

$$\Delta I_m = 4 \left[F\frac{x_m}{2} \right]^{1/2} \left[\frac{-3k^2 J_m \omega^3}{4F_0(1-k^2)^2 m^3} \right]^{-1/2} \ . \tag{3.11}$$

To complete our derivation we need an expression for x_m. Stevens and Sundaram provide an expression for the low-k limit. For the high-k limit we can derive an approximate expression. Using Eq. (2.6) in the integral (3.3) we can write

$$x_m = \frac{x_-}{\pi} \int_{-\pi}^{\pi} d\theta \, \text{sn}^2(u,k)\cos(m\theta) \ . \tag{3.12}$$

We can change the variable of integration if we note that $\theta = \pi[u - E(u,k)]/[K(k) - E(k)]$ [cf. Eqs. (2.4) and (2.7)]. Then we find

$$x_m = \frac{2x_-}{K(k) - E(k)}$$

$$\times \int_0^{K(k) - E(k)} du \, \text{sn}^4(u,k)$$

$$\times \cos \left[\frac{m\pi}{K(k) - E(k)}[u - E(u,k)] \right] \ . \tag{3.13}$$

For $k \approx 1$, $\text{sn}(u,k) \approx \tanh(u)$. If we integrate by parts and let the limit of integration go to infinity [since $K(k) \to \infty$ as $k \to 1$] we obtain

Let us now make another canonical transformation to a new set of action-angle variables, (I, Θ), such that the origin of I is located at $J = J_m$. The generating function for this transformation is

$$\mathcal{F}_2 = (J_m + I) \left[\theta - \frac{\omega}{m} t \right] \ . \tag{3.7}$$

If we keep only the lowest-order terms the new Hamiltonian becomes

$$H = \frac{1}{2} \left[\frac{\partial^2 H_0}{\partial J^2} \right]_{J_m} I^2 - \frac{F}{2} x(J_m)\cos(m\Theta) \ . \tag{3.8}$$

This is just the Hamiltonian for a pendulum. The width, $\Delta I_m \approx \Delta J_m$, of a resonance (trapping region) for a pendulum is

$$\Delta I_m = 4 \left\{ Fx_m \bigg/ \left[2 \left[\frac{\partial^2 H_0}{\partial J^2} \right]_{J_m} \right] \right\}^{1/2} \ . \tag{3.9}$$
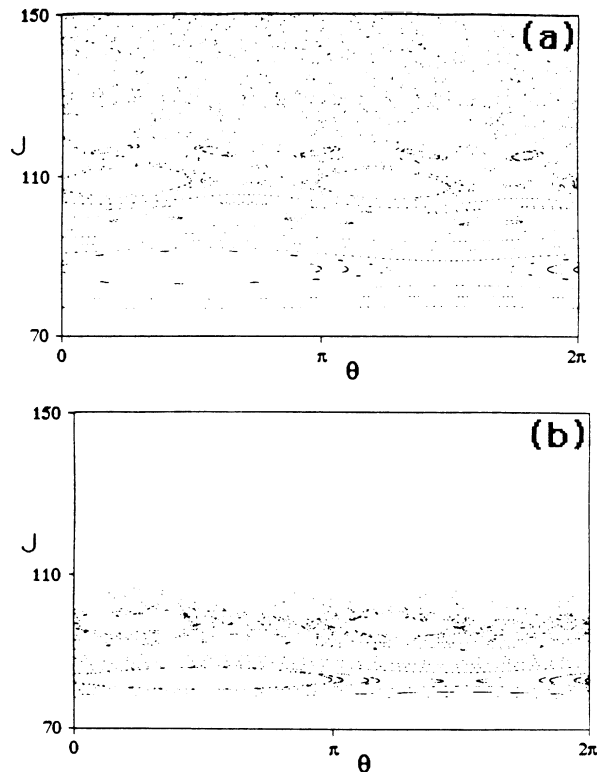
In our case the width can be written

FIG. 4. Numerical strobe plots in action-angle space of the system for frequency $\omega = 1.5 \times 10^{-6}$, microwave field amplitude $F = 10^{-10}$, and two dc field strengths: (a) $F_0 = 10^{-10}$; (b) $F_0 = 10^{-9}$.

$$x_m \approx \frac{-2}{m\pi(F_0)^{1/2}} A(\bar{\omega}) \ , \tag{3.14}$$

where

$$A(\bar{\omega}) = \int_{-\infty}^{\infty} d\theta \left| \frac{\sinh(\theta)}{\cosh^3(\theta)} \right| \sin\{\bar{\omega}[\theta - \tanh(\theta)]\} \ , \tag{3.15}$$

and $\bar{\omega}$ is a dimensionless frequency, $\bar{\omega} = \sqrt{2}\omega/F_0^{3/4}$. $\bar{\omega}$ appears to be the key parameter in determining the behavior of resonances near the separatrix. By complex integration we obtain a power series expansion

$$A(\bar{\omega}) = \frac{\pi}{\sinh[(\pi/2)\bar{\omega}]} \left[\frac{1}{6}\bar{\omega}^2 + \frac{\bar{\omega}^4}{30} + \frac{19\bar{\omega}^6}{7560} \right.$$
$$\left. + \frac{23\bar{\omega}^8}{226\,800} + \cdots \right] \ . \tag{3.16}$$

A plot of $A(\bar{\omega})$ is given in Fig. 5. For small $\bar{\omega}$ (large dc field strengths) or, equivalently, for orbits near the turnover point, $A(\bar{\omega})$ is linear in $\bar{\omega}$. For large $\bar{\omega}$ and large m (small dc field strengths), $A(\bar{\omega})$ approaches the $F_0 = 0$ limit.[1] That is

$$A(\bar{\omega}) \rightarrow 0.411\pi\omega^{-2/3}(F_0)^{1/2} \ . \tag{3.17}$$

The widths of the resonances become narrower as the dc field strength increases, or equivalently, as the resonances become closer to the turnover point ($k = 1$). This is confirmed in Fig. 4. The resonances in the hydrogen atom become narrower but also closer together as the action increases, and eventually overlap. When overlap starts to occur, the dynamics become chaotic as the KAM (Kolmogorov-Arnold-Moser) surfaces break up. Once the motion of the electron becomes chaotic, it may diffuse upward in energy and subsequently ionize. Since overlap depends on the width of the resonances, and therefore the microwave and dc field strengths, we can estimate the threshold field strength needed for the onset of ionization using the widths calculated above.

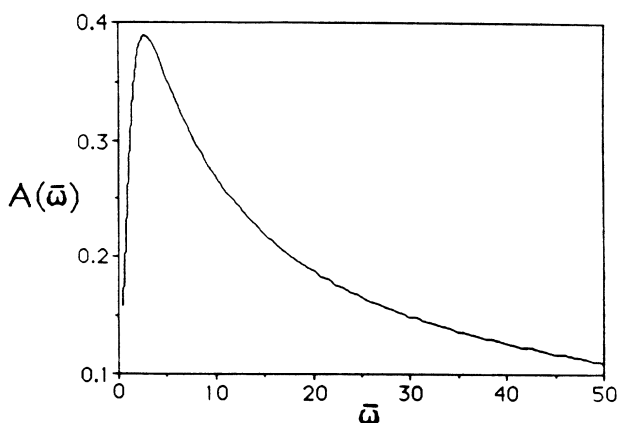We can say that two resonances overlap when the sum

FIG. 5. Plot of the integral $A(\bar{\omega})$ vs the dimensionless frequency $\bar{\omega}$.

of their half-widths is equal to the separation between them:

$$\tfrac{1}{2}(\Delta I_{m+1} + \Delta I_m) = J_{m+1} - J_m \ , \tag{3.18}$$

where, for $k \approx 1$,

$$J_m = \frac{2\sqrt{2}}{3\pi F_0^{1/4}} \left\{ 2 - 4^4 e^{-4m\pi/\bar{\omega}-4} \left[\frac{3}{8} \left[1 + \frac{m\pi}{\bar{\omega}} \right] - \frac{9}{32} \right] \right\} \ . \tag{3.19}$$

Combining Eqs. (3.19) and (3.11) into (3.18) we have an expression for the critical field required for overlap:

$$F = 4F_0 \frac{\bar{\omega}^3}{A(\bar{\omega})} \frac{1}{h^2} \left[\frac{g_1^2}{\bar{\omega}^2} + \frac{g_1 g_2}{2\pi\bar{\omega}} + \frac{g_2^2}{16\pi^2} \right] \ , \tag{3.20}$$

where

$$h = (m+1)e^{-2(m+1)\pi/\bar{\omega}-2} + m e^{-2m\pi/\bar{\omega}-2} \ , \tag{3.21}$$

$$g_1 = (m+1)e^{-4(m+1)\pi/\bar{\omega}-4} - m e^{-4m\pi/\bar{\omega}-4} \ , \tag{3.22}$$

$$g_2 = e^{-4(m+1)\pi/\bar{\omega}-4} - e^{-4m\pi/\bar{\omega}-4} \ . \tag{3.23}$$

Some typical values for overlap are given in Table I. The effect of the dc field is to give a slightly lower threshold microwave field strength for overlap, and hence ionization. The accuracy of the pendulum approximation is suspect, however, for resonances too close to the turnover.[6,7] Even though the pendulum approximation overestimates the resonance zones, the critical field for overlap, obtained from strobe plots, is actually less than those given in Table I by about a factor of 2. The reason for this is that higher-order resonances were not taken into account. These higher-order resonances, lying between the primary resonances, grow rapidly when the primary resonances are about to overlap and help to destroy the KAM surfaces that separate the primary resonances.

IV. ONSET OF CHAOS—
THE STANDARD-MAP APPROACH

We will now determine the onset of chaos using the standard map. First we derive a whisker map[5] which maps the energy and the phase of the field from one

TABLE I. Critical values for island overlap using the Chirikov overlap criterion for typical dc field strengths found in experiments (Ref. 2). For all cases $\omega = 1.5 \times 10^{-6}$.

m	F_0	F
1 and 2	10^{-9}	4.0×10^{-10}
	10^{-10}	5.5×10^{-10}
	10^{-11}	5.6×10^{-10}
2 and 3	10^{-9}	9.3×10^{-11}
	10^{-10}	1.5×10^{-10}
	10^{-11}	1.6×10^{-10}
3 and 4	10^{-9}	2.8×10^{-11}
	10^{-10}	1.0×10^{-10}
	10^{-11}	1.2×10^{-10}

period of the orbit to the next. We restrict our attention to orbits in the neighborhood of the separatrix. Let us first generalize Eq. (1.1) to include a phase ϕ in the microwave term

$$H = \tfrac{1}{2}p^2 - \frac{1}{x} - F_0 x - Fx \cos(\omega t + \phi) . \tag{4.1}$$

We next introduce a value for the energy, W_n ($W = |E_0|$), and the phase ϕ_n at the end of the nth period of the orbit. The change in W_n and ϕ_n from one period of the orbit to the next is given by

$$\begin{bmatrix} W_{n+1} \\ \phi_{n+1} \end{bmatrix} = \begin{bmatrix} W_n + \Delta H_0 \\ \phi_n + \Delta \phi \end{bmatrix} , \tag{4.2}$$

where ΔH_0 is the change in the unperturbed energy during one period of the orbit. In the neighborhood of the separatrix, where the period of the orbit becomes infinite, the change in the energy during one period of the orbit can be written

$$\Delta H_0 = \int_{-\infty}^{\infty} dt \left[\frac{dH_0}{dt} \right]_{sx}$$

$$= -F \int_{-\infty}^{\infty} dt \, p_{sx}(t) \cos(\omega t + \phi) , \tag{4.3}$$

where

$$p_{sx}(t) = \frac{2\sqrt{2} F_0^{1/4}}{\sinh(2\theta)} \tag{4.4}$$

with

$$\theta - \tanh(\theta) = \frac{F_0^{3/4} t}{\sqrt{2}} . \tag{4.5}$$

Performing the integration we obtain

$$\Delta H_0 = \frac{2FA(\bar{\omega})}{(F_0)^{1/2}} \sin(\phi) \tag{4.6a}$$

for $F_0 \neq 0$ [$A(\bar{\omega})$ is defined in Eq. (3.15)] and

$$\Delta H_0 = F\Gamma(\tfrac{2}{3}) \frac{2}{\sqrt{3}} \left[\frac{3}{\sqrt{2}\omega} \right]^{2/3} \sin(\phi) \tag{4.6b}$$

for $F_0 = 0$, where $\Gamma(\tfrac{2}{3})$ is the gamma function. The period of an orbit near the separatrix (potential turnover) is approximately

$$\tau = \frac{1}{\sqrt{2} F_0^{3/4}} \left[\ln \left[\frac{64(F_0)^{1/2}}{W} \right] - 4 \right] . \tag{4.7}$$

In the limit of $F_0 \to 0$, the period becomes

$$\tau = \frac{\pi}{\sqrt{2} W^{3/2}} . \tag{4.8}$$

The change in phase is simply $\Delta \phi = \omega \tau$. Our mapping is then

$$\begin{bmatrix} W_{n+1} \\ \phi_{n+1} \end{bmatrix} = \begin{bmatrix} W_n + \dfrac{2FA(\bar{\omega})}{(F_0)^{1/2}} \sin(\phi_n) \\[2mm] \phi_n + \dfrac{\bar{\omega}}{2} \left[\ln \left[\dfrac{64(F_0)^{1/2}}{W_{n+1}} \right] - 4 \right] \end{bmatrix} \tag{4.9a}$$

for the case $F_0 \neq 0$ and for the case $F_0 = 0$ we find

$$\begin{bmatrix} W_{n+1} \\ \phi_{n+1} \end{bmatrix} = \begin{bmatrix} W_n + F\Gamma(\tfrac{2}{3})\dfrac{2}{\sqrt{3}} \left[\dfrac{3}{\sqrt{2}\omega} \right]^{2/3} \sin(\phi_n) \\[2mm] \phi_n + \dfrac{\pi\omega}{\sqrt{2} W_{n+1}^{3/2}} \end{bmatrix} . \tag{4.9b}$$

For the case $F_0 = 0$, this mapping is equivalent to the Kepler map derived by Casati et al.[8] The Kepler map derived in Ref. 8, however, was derived under the more general condition $\omega\tau > 2\pi$. The resonance zones for these mappings occur at the fixed points where $\Delta\phi = 2m\pi$. We then obtain for the location of the resonances

$$W_m = 64(F_0)^{1/2} e^{-4(m\pi/\bar{\omega}+1)} , \tag{4.10a}$$

for $F_0 \neq 0$ and

$$W_m = \frac{1}{2} \left[\frac{\omega}{m} \right]^{2/3} \tag{4.10b}$$

for $F_0 = 0$. These mappings are only strictly valid near the separatrix ($k = 1$ for the case $F_0 \neq 0$). Figure 6 shows a comparison of the phase-space orbits given by the whisker map with strobe plots (Poincaré surfaces of section) obtained numerically using Hamilton's equations of motion obtained from the Hamiltonian in Eq. (1.1). In Fig. 6(a), $k = 0.60 - 0.84$, so the mapping is not bad con-
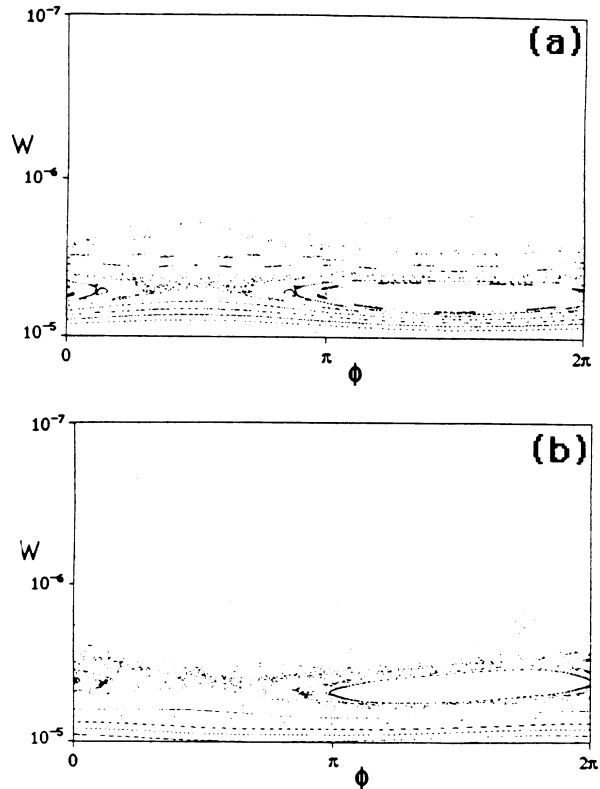

FIG. 6. (a) Numerical strobe plot of energy vs phase of the field ($\phi = \omega t$) for $\omega = 1.5 \times 10^{-6}$, $F_0 = 10^{-9}$, $F = 4.6 \times 10^{-11}$, and modulus $k = 0.60 - 0.84$ ($W = |E_0| = 10^{-5} - 10^{-7}$). (b) The whisker map for the same system.

sidering that this is outside the range of its validity. Figure 7 shows a mapping closer to the separatrix ($k = 0.84 - 0.97$). The agreement in the size and location of the resonances as well as the onset of chaos is remarkably good.

Let us now derive the standard map from the whisker map in Eqs. (4.9). We linearize the whisker map around a particular resonance to obtain an expression for the threshold field strength required for resonance overlap. Let us define

$$I = (W - W_m) \left| \frac{d \Delta \phi}{dW} \right|_{W_m} . \tag{4.11}$$

We then arrive at the standard map

$$\begin{bmatrix} I_{n+1} \\ \phi_{n+1} \end{bmatrix} = \begin{bmatrix} I_n + K \sin(\phi_n) \\ \phi_n + I_{n+1} \end{bmatrix} , \tag{4.12}$$

where K is defined

$$K = \overline{\omega} \frac{F}{F_0} \frac{A(\overline{\omega})}{64} e^{4(m\pi/\overline{\omega}+1)} \tag{4.13a}$$

for $F_0 \neq 0$ and

$$K = 48.5 F \omega^{-4/3} m^{5/3} \tag{4.13b}$$

for $F_0 = 0$. The standard map has been extensively studied[5] and is known to become globally chaotic when $K \approx 1$. If we set $K = 1$ in Eqs. (4.13), we obtain the following estimate for the threshold field strength required for overlap:

$$F = \frac{64 F_0}{\overline{\omega} A(\overline{\omega})} e^{-4(m\pi/\overline{\omega}+1)} \tag{4.14a}$$

for $F_0 > 0$, and

$$F = 0.02 \omega^{4/3} m^{-5/3} \tag{4.14b}$$

for $F_0 = 0$. Both of these expressions have been confirmed by comparison with strobe plots for a wide range of parameters.

We can compare Eqs. (4.14a) and (4.14b) with previously published results. Equation (4.14b), which is essentially the same result derived by Casati et al.,[8] agrees with the threshold derived by Jensen[1] except for the numerical constant. Our numerical constant, being more than a factor of 2 smaller than that of Jensen, is in closer agreement with numerical results. The reason for this is that the standard-map approach takes higher-order resonances into account. Equations (4.14), for the same reason, provide a better estimate than the ones we derived in Sec. III. Equation (4.14a) agrees with the results obtained by Reichl and Zheng[6] for the double-well potential in the low-ω limit. This is not too surprising since both potentials are quadratic near the turnover point for small ω.

V. CONCLUSION

We have used two approaches to derive the critical field strength required for resonance island overlap for a hydrogen atom driven by both a dc and a microwave
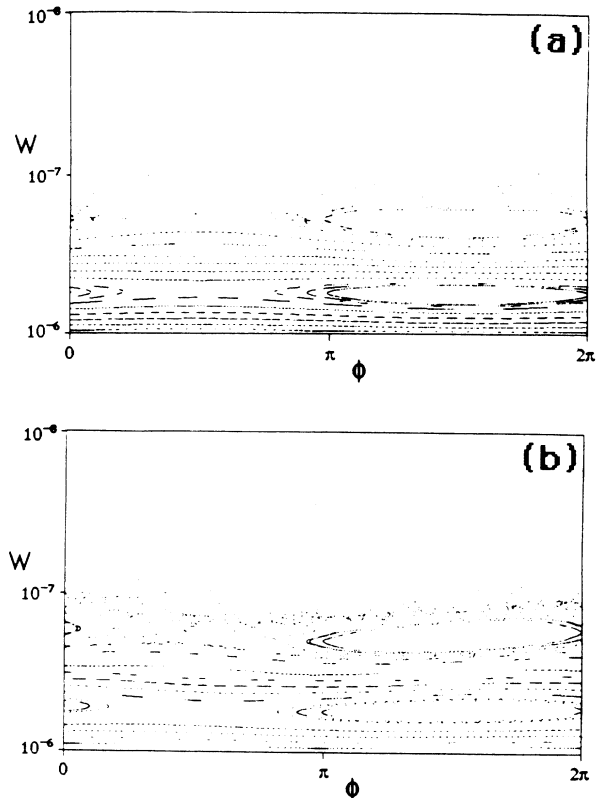

FIG. 7. (a) Numerical strobe plot of energy vs phase of field ($\phi = \omega t$) for $\omega = 1.5 \times 10^{-6}$, $F_0 = 10^{-9}$, $F = 1.97 \times 10^{-12}$, and modulus $k = 0.84 - 0.97$ ($W = |E_0| = 10^{-6} - 10^{-8}$). (b) The whisker map for the same system.

field. The first approach uses the first-order Chirikov overlap criterion and gives a crude (within a factor of 2) estimate for the critical field strength. The second approach uses the standard map which is obtained by linearizing a whisker map around a desired resonance. For the case of no static field, our map is equivalent to the Kepler map derived by Casati et al.[8] Although Casati et al. include corrections for a small static field in their mapping, we have derived a result for an arbitrary static field.

The standard-map approach gives more accurate values when compared with numerical experiments. This is due to the inclusion of higher-order resonances. These higher resonances can be included in the Chirikov approach. This has been done[9,10] for the case of no static field, and the results compare well with the standard-map approach. As a final point, we should emphasize that the mapping approach used here is valid only near the potential turnover.

ACKNOWLEDGMENTS

[1]R. V. Jensen, Phys. Rev. A **30**, 386 (1984).
[2]J. N. Bardsley, B. Sundaram, L. A. Pinnaduwage, and J. E. Bayfield, Phys. Rev. Lett. **56**, 1007 (1986).
[3]K. A. H. van Leeuwen, G. v. Oppen, S. Renwick, J. B. Bowlin, P. M. Koch, R. V. Jensen, O. Rath, D. Richards, and J. G. Leopold, Phys. Rev. Lett. **55**, 2231 (1985).
[4]M. J. Stevens and B. Sundaram, Phys. Rev. A **36**, 417 (1987).
[5]B. V. Chirikov, Phys. Rep. **52**, 263 (1979).

[6]L. E. Reichl and W. M. Zheng, Phys. Rev. A **30**, 1068 (1984).
[7]W. A. Lin and L. E. Reichl, Phys. Rev. A **31**, 1136 (1985).
[8]G. Casati, I. Guarneri, and D. Shepelyanski, IEEE **24**, 1420 (1988).
[9]N. B. Delone, V. P. Krainov, and D. L. Shepelyanski, Usp. Fiz. Nauk **140**, 355 (1983) [Sov. Phys.—Usp. **26**, 551 (1983)].
[10]J. G. Leopold and D. Richards, J. Phys. B **18**, 3369 (1985).